A multivariate analysis of the association between corticostriatal functional connectivity and psychosis-like experiences in the general community.

Sara Maria Pani *[1], Kristina Sabaroedin, Jeggan Tiego, Mark A. Bellgrove, Alex Fornito

Turner Institute for Brain and Mental Health, School of Psychological Sciences, and Monash Biomedical Imaging, Monash University, 770 Blackburn Rd, VIC 3800, Australia

Keywords: Psychosis; fMRI; Connectivity; Basal ganglia; Caudate; Prefrontal Cortex.

[1] Permanent Address: Department of Biomedical Sciences, Department of Medical Sciences and Public Health, PhD Program in Neuroscience, University of Cagliari, Cittadella Universitaria – 09042, Monserrato (CA) - Italy

* +39 3405683227, email: saramariapani@gmail.com

Abstract

Dysfunction of dorsal corticostriatal (CST) circuitry is thought to play an important role in psychosis. Here, we use multivariate analysis to characterize covariance between CST functional connectivity (FC) and psychosis-like experiences (PLEs) in non-clinical individuals. In 353 healthy adults (155males), we use partial least squares (PLS) to identify latent variables (LV) describing covariance between seven PLE questionnaire measures and functional connectivity estimated between each of six striatal seed regions and the rest of the brain using multiband resting-state fMRI. Hypothesis-driven PLS of the dorsal caudate (DC) seed identified one significant LV, accounting for 23.88% of covariance, with loadings from nearly all PLE subscales. Cortical regions implicated in this LV comprise anterior cingulate and left dorsolateral prefrontal cortex. Lower connectivity between these cortical areas and the DC seed was associated with more severe PLEs. Using multivariate modelling, we identified an association between dorsal CST connectivity and PLEs in the general community that implicates similar brain regions to those identified in patient groups. Our results highlight that the severity of both positive/negative symptom-like PLEs is related with functional coupling between the DC and dorsolateral PFC, suggesting this neural circuit may play a role in mediating risk for general psychosis-related psychopathology.

1. Introduction

Psychotic symptoms can vary in severity along a continuum that extends from isolated unusual experiences to clinical disorders such as schizophrenia (Grant et al., 2018; Kelleher and Cannon, 2011; R. et al., 2000; van Os et al., 1999). In the subclinical range, psychosis-like experiences (PLEs) (Unterrassner et al., 2017) are thought to represent attenuated forms of typical positive symptoms, such as hallucinations and delusions, but they can also include negative-like symptoms(Stefanis et al., 2002; Verdoux and van Os, 2002). PLEs are quite common in the general population, with a prevalence of up to 8% (Van Os et al., 2009). People reporting higher levels of PLEs are at increased risk of schizophrenia-spectrum disorders, suggesting that PLE severity may relate to one's vulnerability to clinical disorder (Kelleher and Cannon, 2011). The potential for PLEs to index liability for psychosis has driven a growing interest in understanding subclinical symptoms in the general community (Ettinger et al., 2014; Grant et al., 2018; Tandon et al., 2012). Indeed, the continuum model is supported by behavioral, genetic, cognitive, and neuroimaging evidence of continuities between clinical and subclinical phenomena (Cannon et al., 2002; Ettinger et al., 2012; Lee et al., 2012; R. et al., 2000; Sabaroedin et al., 2019; Van Os et al., 2009). PLE severity in non-clinical samples correlates with variations in the structure and function of brain systems implicated in psychotic disorders (e.g., frontotemporal, default mode, cingulo-opercular systems)(Ettinger et al., 2012; Garrity et al., 2007; Satterthwaite et al., 2015; Sheffield et al., 2016), and with measures of the integrity of their interconnecting white matter pathways (Jacobson et al., 2010; Skudlarski et al., 2013).

Corticostriatal (CST) circuits have been identified as playing an important role in the emergence of psychotic symptoms. These circuits comprise topographic connections from prefrontal cortex to striatum, with feedback loops passing through the pallidum and thalamus (Haber, 2016; Simpson et al., 2010). Two circuits implicated in psychosis include a ventral, so-called limbic system, which connects orbitofrontal cortex, medial prefrontal cortex, and limbic structures with the ventral striatum, and a dorsal, so-called associative system, which connects the dorsolateral prefrontal cortex with the dorsal striatum (Dandash et al., 2017; Draganski et al., 2008; Grace, 2016; Haber, 2016). The function of the striatum is heavily modulated by dopamine, and a series of reports indicate that this neurotransmitter is most strongly elevated in the dorsal striatum of patients with schizophrenia, their unaffected relatives, and individuals with an at-risk mental state

(ARMS) for psychosis(Howes et al., 2009; Huttunen et al., 2008; Study, 2010). Studies of striatal functional connectivity have also found decreased functional coupling between the dorsolateral prefrontal cortex (PFC) and dorsal striatum and putamen in first-episode psychosis-patients, their unaffected first-degree relatives, and individuals with ARMS (Dandash et al., 2014; Fornito et al., 2013), as well as in first-episode mania patients with psychotic symptoms (Dandash et al., 2018). These lines of evidence suggest that dorsal CST connectivity may play a critical role in in the emergence of psychotic symptoms across traditional diagnostic categories. Additionally, reduced dorsal CST coupling is correlated with the severity of positive and negative symptoms in ARMS individuals when the thalamus, rather than striatum, is used as a seed for connectivity analysis (Anticevic et al., 2015; Dandash et al., 2014; Fornito et al., 2013) .

Complimenting findings in clinical samples, we recently reported evidence that functional connectivity of dorsal CST circuits correlated with the severity of PLEs in a non-clinical sample of healthy individuals living in the general community (Sabaroedin et al., 2019). PLEs were quantified using 12 subscales taken from 7 different questionnaires, and principal component analysis (PCA) was used to summarize the data, wherein two components described shared variance between measures of (1) PLEs related to positive symptoms; and (2) PLEs related to negative symptoms. The analysis revealed that higher levels of positive PLEs were associated with lower functional connectivity between dorsal caudate and anterior cingulate cortex, and between dorsorostral putamen and dorsolateral prefrontal cortex. Although our findings in the non-clinical sample support a general involvement of dorsal CST circuitry across the psychosis spectrum, the spatial topography of the circuits correlating with PLEs diverged from the areas implicated in studies of clinical and high-risk groups(Dandash et al., 2017; Fornito et al., 2013)(see Sabaroedin et al. (Sabaroedin et al., 2019), *Figure 3*). More specifically, where dysconnectivity between the dorsal caudate and dorsolateral PFC has been consistently implicated in clinical samples(Dandash et al., 2017, 2014; Fornito et al., 2013), positive PLEs in the non-clinical sample were associated with functional connectivity between the dorsal caudate and anterior cingulate cortex. One potential reason for this discrepancy is that the dimension reduction of PLE subscales via PCA in the non-clinical group emphasized only common modes of shared variance across measures and may have masked correlations between functional connectivity and specific aspects of PLEs.

Here, we apply partial least squares (PLS) analysis to the same cohort studied in Sabaroedin et al. (Sabaroedin et al., 2019) to uncover latent dimensions describing covariance between corticostriatal functional connectivity and the 12 subscales used to measure PLEs. This analysis allows a fine-grained examination of the covariation between functional connectivity and PLE scores, thus providing a more complete picture of the relation between the two. We hypothesized that this approach would reveal an association between positive PLE severity and functional connectivity between the dorsal caudate and dorsolateral prefrontal cortex, thus mapping an association between brain and behavior that more closely aligns with the circuit implicated in clinical samples.

2. Materials and methods

2.1. Participants

Data were collected as a part of a larger genetics study that required participants to have all four grandparents of European descent. The 672 participants recruited (274 males; age range = 18–50 years old, mean [SD] age = 23.2 [4.89]) from the general community completed an online battery of PLEs measures. All participants had no personal history of psychiatric or neurological illness, no significant drug use and were right-handed. Each participant voluntarily confirmed his/her willingness to participate, providing written informed consent after having been informed of all aspects of the study. The study was conducted in accordance with the Monash University Human Research Ethics Committee (reference number 2012001562). A total of 379 participants with complete PLEs measures underwent our resting-state fMRI protocol, with data for 353 participants (155 males; median age [range] = 22 [18–50 years]) being retained for final analysis following exclusions for imaging artifacts, poor scan quality, and excessive head motion (see Sabaroedin et al. (Sabaroedin et al., 2019) for details). Here, we present analyses of this final sample.

2.2. Measures of psychosis-like experiences

Seven psychometrically validated self-report measures of subthreshold psychotic symptoms were used, allowing us to sample a wide range of variation in PLEs. The scales included the Community Assessment of Psychotic Experience (CAPE)(Mossaheb et al., 2012), four Chapman Scales(Chapman and Chapman, 1980) measuring magical ideation(Eckblad and Chapman, 1983), perceptual aberration(Chapman et al., 1978), and

social and physical anhedonia(Chapman et al., 1976), the short-form Oxford Liverpool Inventory of Feelings and Experiences (sO-LIFE) (Fonseca-Pedrero et al., 2015)and the Peters Delusion Inventory (PDI-21)(Peters et al., 2004) (a complete description of the above measures can be found in the Supplemental Information). The battery produced a total of 272 items spanning 12 subscales. These subscales, the questionnaires from which they were derived, and descriptive statistics (*n*=353) are listed in Table 1.

2.3. Neuroimaging data acquisition and pre-processing

For each participant we acquired multiband resting-state echo-planar images (EPI; 620 volumes, 754 milliseconds repetition time, 3mm isotropic voxels) and anatomical T1-weighted scans (1mm isotropic voxels) using 3T Siemens Skyra MRI scanner equipped with a 32-channel head coil, located at the Monash Biomedical Imaging facility, Melbourne, Australia.

A total of 620 functional volumes, each with 42 slices, were acquired per subject using an interleaved acquisition with the following parameters: repetition time (TR) of 754 milliseconds, echo time (TE) of 21 milliseconds, flip angle of 50°, multiband acceleration factor of 3, field of view (FOV) of 190mm, slice thickness of 3mm, and 3mm isotropic voxels. For each subject were also acquired anatomical T1-weighted images using a 3-dimensional magnetic-prepared rapid gradient echo sequence. For each subject's T1-weighted images were acquired a total of 192 slices using an ascending acquisition with the following parameters: TR of 2300 milliseconds, TE of 2.07 milliseconds, flip angle of 9°, FOV of 256mm, and voxel size of $1mm^3$.

The EPI images were processed using the following steps. First, we performed basic pre-processing in FSL FEAT (Woolrich et al., 2001), which includes removal of the first four volumes, rigid-body head motion correction, 3mm spatial smoothing, and a highpass temporal filter (75 seconds cut-off). Second, artefactual and other noise components were removed from the data using FSL-FIX (Griffanti et al., 2014; Salimi-Khorshidi et al., 2014), which was trained using an independent dataset of 25 individuals scanned with identical imaging parameters. This independent component analysis-based denoising approach uses the training data to automatically classify noise components (signal contributions from head motion, sources of scanner and physiological noise, white matter, cerebrospinal fluid signals) for removal of from the data. As

nuisance regressors, we used i) the time courses of the components labelled as noise, ii) 6 standard head motion parameters (3 rotation, 3 translation) in addition to their squares and derivatives, iii) the averaged signal taken from a mask of the entire brain (i.e., a "global" signal) along with the first derivatives and squares of each. The denoised data were then spatially normalized to the MNI152 template via ANTs (version 2.2.0)(Avants et al., 2011) following a three-step method that comprised the registration of the mean realigned functional scan to the skull-stripped high resolution anatomical scan via rigid-body registration; spatial normalization of the anatomical scan to the MNI template via a nonlinear registration; and normalization of functional scan to the MNI template using a single transformation matrix that concatenates the transforms generated from the precedent steps. The spatially normalized functional images were subsequently spatially smoothed with a 6mm full-width half maximum Gaussian kernel using AFNI (version 16). In line with past work(Parkes et al., 2018), the data were subjected to rigorous quality control for motion artefacts after pre-processing, and residual motion contamination was minimal. Full details can be found in Sabaroedin et al. 2019 (Sabaroedin et al., 2019).

2.4. Definition of seed regions of interest

As per past work(Dandash et al., 2014; Fornito et al., 2013; Sabaroedin et al., 2019) we seeded six striatal regions-of-interest (ROI)(figure SF8) in each hemisphere using a 3.5mm radius spheres, following the method proposed by Di Martino et al(Di Martino et al., 2008). Three ROIs were seeded along a dorsoventral axis for the caudate, comprising the dorsal caudate (DC; x = ±13, y = 15, z = 9), the superior ventral caudate (x = ±10, y = 15, z = 0), and the inferior ventral caudate/nucleus accumbens (x = ±9, y = 9, z = -8). For the putamen, we seeded three ROIs along a similar axis, incorporating the dorso-caudal putamen (DCP; x = ±28, y = 1, z = 3), the dorso-rostral putamen (DRP; x = ±25, y = 8, z = 6), and the ventro-rostral putamen (VRP; x = ±20, y = 12, z = -3). The dorsal CST seeds incorporate DC, DRP, and DCP. The ventral CST seeds encompass the inferior ventral caudate/nucleus accumbens, superior ventral caudate, and VRP. We used the mean time series of each region to generate seed-related functional connectivity maps.

2.5. Functional connectivity analysis

As described in past work (Dandash et al., 2014; Sabaroedin et al., 2019), subject specific first-level analysis was performed using SPM8. For each subject, whole-brain functional connectivity maps of each striatal ROI were estimated by entering the time series from the six striatal ROIs into a general linear model. Left and right hemispheres were modelled separately, yielding a pair of functional connectivity maps for each striatal ROI. The unthresholded contrast images for both hemispheres were then entered into a PLS analysis.

2.6. PLS analysis.

PLS is a multivariate statistical technique that combines PCA-style dimensionality reduction with linear regression. First introduced to functional neuroimaging by McIntosh et al.(McIntosh et al., 1996), it is well-suited to uncovering multivariate associations between brain imaging and behavioral measures (Krishnan et al., 2011). The analysis examines the covariation among two or more "blocks" of variables (McIntosh et al., 1996). In our case, the blocks represent seed-related functional connectivity and PLEs scores, and the final aim is to obtain a new set of variates that represent linear combinations of each block' variables that covary, at the maximal degree, with each other.

In this study we used the variant *Regular Behavior PLS* analysis implemented in PLS toolbox (McIntosh et al., 1996) written in Matlab (The MathWorks, Inc., Natick, Massachusetts, US), to analyze the relationship between the 12 PLEs subscales, age and sex, and striatal functional connectivity. We ran a separate PLS analysis for each seed region, including the maps for left and right seed-related FC as different conditions (left: condition 1, right: condition 2). The PLS approach we used here is outlined in detail in (Krishnan et al., 2011; McIntosh et al., 1996). We started with two sets of variables, represented respectively by: (i) seed-to-brain functional connectivity maps; and (ii) PLE subscale scores, with the nuisance covariates age and sex. The sets of variables were organized in two different matrices: X for the brain activity, and Y for behavioral and demographic data (age and sex). The matrix X consists of i observations and j voxels, where each voxel encodes functional connectivity with a given seed region. Voxels are ordered such that all left hemisphere voxels are listed first, followed by all right hemisphere voxels, representing two conditions in the PLS. The matrix Y consists of i observations and k behavioural measures and (optionally) nuisance covariates. The two matrices were centered and normalized within each condition, and a matrix of correlations was computed separately for each condition. The two condition matrices of correlations were combined into a

single matrix referred as the cross-block correlation matrix R, which contains the correlation of each of the j voxels in X with each of the k behavioural/demographic measures in Y, within each of the conditions.

The cross-block correlation matrix R was subjected to a singular value decomposition (SVD), which produced a set of independent (orthogonal) latent variables (LV) / singular vector pairs. Each pair is associated with a singular value that reflects the covariance between the paired LVs (i.e., the functional connectivity LV, comprising brain scores, and the PLE, or behavioral LV), ranked by the proportion of squared cross-block covariance explained. Each LV constitutes a distinct weighted pattern of functional connections and PLE subscale scores that covary, in an ideal manner, with each other. One member of an LV pair is composed of saliences/weights corresponding to each measure in the functional connectivity block, and the other member is composed of saliences for each measure in the behavioral measures block. Thus, considering a given pair of variables, the saliences within one of them point out, basically, which measurements are driving the covariation with the other corresponding latent variable. The statistical significance of each LV is determined using *permutation tests* (Krishnan et al., 2011). The resulting p-values quantify the number of times the permuted singular values exceeded the observed singular values. In our study, we used 5000 permutations, performed by randomly reordering the rows of the original data matrix X. As our primary hypothesis concerned the dorsal caudate, LVs in this analysis were declared statistically significant at $p < 0.05$. All other results were declared significant if they survived Bonferroni-correction over the six seeds ($p < 0.008$).

We also assessed the reliability of brain saliences (voxel weights on the brain LV) via bootstrapping (Krishnan et al., 2011). A total of 1000 bootstrap samples were obtained by randomly resampling with replacement the X matrix within each condition. The SVD was then performed on the resampled data matrices to generate new saliences (weights) which were projected into the space of the original analysis and used to estimate the standard error of each weight, representing a measure of stability. For each voxel was then calculate a bootstrap ratio (BSR) by dividing the weight from the singular vector by its bootstrap-estimated standard error. The BSR ratio is considered equivalent to a z-score when the bootstrap distribution is approximately normal(efron, B Tibshirani, 1986), and if the ratio of salience over its standard error is greater than 2, the salience is considered reliable. The BSR ratio results are thresholded, by default, at values

corresponding to the 95% confidence interval. The resulting voxelwise BSR maps may thus reveal voxels in which functional connectivity with the seed region contributed strongly and reliably to the multivariate pattern identified in a given LV. Permutation testing and bootstrapping ensured robustness and avoided over-fitting.

3. Results

We applied PLS to explain the covariance between left and right striatal seed-related FC and 14 behavioral/demographic measures, comprising 12 PLEs subscales, age, and sex. A separate PLS was run for each of the six seeds, with hemisphere included as a condition within each analysis (left, condition 1; right, condition 2).

3.1. Associations between dorsal caudate functional connectivity and PLEs

Our hypothesis-driven PLS of the DC seed identified LV1 as statistically significant, accounting for 23.88% of cross-block covariance, with a singular value of 56.94 and p=.019 (see Supplemental SF1). Figure 1a shows that this LV pair was characterized by uniform loadings across nearly all PLE subscales on both left and right DC-related FC, with minimal contributions from age and sex. There was some evidence for lower contributions from negative PLE scales; namely, the CAPE negative and Chapman social and physical anhedonia scales, and sO-LIFE introvertive anhedonia. However, the 95% confidence intervals of the correlations between these scales and brain scores on LV1 did not cross zero, suggesting that they still make a significant contribution. Thus, this LV describes an association between DC-related FC and general PLE severity. Across all PLE scales, more severe experiences were associated with lower brain scores. Example scatterplots for two representative positive and negative PLE scales are shown in Supplemental Figure SF2.

Figure 1b shows the bootstrap image obtained from the PLS analysis, which maps voxels that reliably contribute to the significant LV (see ST1 for cluster sizes and peak coordinates for the maps in panel 1b). In other words, this map identifies voxels where functional connectivity with the DC seed is associated with the multivariate profile of PLE subscale scores shown in Figure 1a.

The pattern is strongly expressed in the caudal and rostral anterior cingulate cortex, medial prefrontal cortex, left dorsolateral prefrontal cortex and dorsomedial thalamus, right pallidum, and posterior right cerebellum.

These brain regions express a negative correlation between PLEs scores and DC-related FC; i.e., higher scores on PLE scales are associated with lower FC. This pattern is reversed in areas of bilateral occipital and parietal cortex, where higher PLEs scores are associated with higher DC-related FC (see Figure 1, panel b).

3.2. Associations between PLEs and the functional connectivity of other striatal seed regions

No other LVs passed our Bonferroni-corrected threshold for significance (α=0.008) when considering the remaining striatal seed regions (i.e., dcPT, drPT, vrPT, VSi, VSs). Three LVs, all involving the putamen, surpassed a p<.05, uncorrected threshold: two LVs were related to the dcPT seed and one LV was related to the vrPT seed.

The two dcPT-related seeds accounted for 59.5% and 46.7% of the cross-block covariance (p=.005 and p=.048, respectively; Figure SF3). The first LV shows comparable PLEs loadings across both hemispheres, with a behavioral profile characterized by similar loadings across most positive PLEs subscales, with attenuated loadings for anhedonia-related and CAPE negative scales (Figure SF4, panel a). The bootstrap ratio map revealed reliable contributions from dcPT-related FC in anterior and posterior cingulate cortices, dorsolateral prefrontal cortex, right superior parietal cortex, visual cortices, pallidum, and bilateral cerebellum (Figure SF4, panel b, ST2).

LV2 for the dcPT seed described a profile in which negative PLEs scales consistently loaded on both left and right seed-related FC, whereas positive PLEs scales showed smaller correlations which were negative in the left and positive in the right hemisphere (Figure SF5, panel a). The bootstrap ratio image identified reliable contributions from voxels in left medial prefrontal cortex, right orbitofrontal cortex, dorsal anterior and ventral posterior cingulate cortex, thalamus, sensorimotor cortex, right paracentral lobule, and right cerebellum (Figure SF5, panel b, ST3).

The vrPT-related LV accounted for 22.5% of the cross-block covariance (p=.043; Figure SF6). It was characterized by higher loadings from positive PLEs scales, particularly for right-hemisphere seed-related FC (Figure SF7, panel a). Voxels contributing reliably to this pattern were located in orbitofrontal right cortex, mid-cingulate cortex, medial prefrontal and dorsolateral prefrontal cortices, inferior precentral sulcus and visual and somatosensory cortex (see SF7, panel b, ST4).

4. Discussion

Corticostriatal abnormalities are apparent from the earliest stage of psychosis, with patients, their unaffected-relatives, and ARMS individuals showing similar changes, suggesting that dorsal CST dysfunction may represent a risk phenotype for psychotic disorders (Dandash et al., 2017; Fornito et al., 2013). Dysconnectivity of dorsal CST circuitry also correlates with symptom severity in patient groups (Dandash et al., 2014; Fornito et al., 2013) and subclinical variation in positive PLEs in a healthy community sample (Sabaroedin et al., 2019), although the specific regions implicated in the PLE analysis differed from those identified in clinical samples. Here, we applied PLS to identify multivariate associations between 12 PLE measures and CST FC in a non-clinical sample. We found that functional connectivity of the dorsal caudate was associated with PLE severity across both positive-like and negative-like symptom domains, with PLS identifying a significant LV with comparable loadings from all PLE subscales. Critically, the cortical regions implicated in this DC-related LV include regions of anterior cingulate cortex, as per the results of our prior univariate analysis in this sample (Sabaroedin et al., 2019), as well as areas of left dorsolateral PFC, which more closely align with areas implicated as dysfunctional in clinical samples. Paralleling the clinical findings, lower FC between these cortical areas and the DC seed was associated with more severe PLEs in the current study. A summary of the anatomical consistency of the circuits implicated in the current work and past studies of clinical cohorts is provided in Figure 2.

These results suggest that dorsal circuit FC tracks symptom severity across a wide spectrum of clinical and subclinical severity, and that the spatial correspondence between the specific circuit elements involved is closer than suggested in Sabaroedin et al's (Sabaroedin et al., 2019) (2019) analysis. Indeed, it seems that these earlier results, which did not implicate dorsolateral PFC, may have been driven by the different analysis method used, in which PLE scales were subjected to a PCA before being correlated with FC. In this way, the approach of Sabaroedin et al. mapped areas associated with common dimensions of variance specifically in positive PLE scores. The present findings indicate that DC-dorsolateral PFC FC is implicated when considering a dimension of variance *common across all PLE scales*, encompassing both positive-like and negative-like symptoms. It may thus be related to a more generalized component of schizophrenia risk. Consistent with this view, work in first episode patients has reported that functional connectivity between the

DC and left dorsolateral PFC is associated with the severity of both positive and negative symptoms(Fornito et al., 2013). (Fornito et al., 2013). Given that the LV identified in our analysis of DC-related functional connectivity included comparable loadings across all scales, it is possible that the multivariate FC profile identified in this analysis is associated with a more general psychopathology factor, sometimes referred to as the *p*-factor (Caspi and Moffitt, 2018). A more comprehensive investigation of non-psychosis-like symptoms would thus help to determine the specificity of our findings.

We also found suggestive evidence for associations between the FC of other striatal seeds and PLE severity. Again, the dorsal circuit was predominant, two LVs were identified for the dcPT and only one implicated the ventral system. The associations between dorsocaudal putamen FC and PLE severity involved areas that have been identified as dysfunctional in patients, such as orbitofrontal cortex and thalamus, pallidum, anterior cingulate cortex, and dorsal prefrontal cortex(Fornito et al., 2013, 2011, 2008; Haber and Knutson, 2010; Reid et al., 2010; White et al., 2010; Woodward and Heckers, 2016) as well as sensorimotor and visual cortices. The cortical regions implicated in the vrpT-related associations with PLE severity included regions of mid-cingulate cortex, generally deemed as common boundary between cognition and motor control, the orbitofrontal cortex, and medial and dorsolateral prefrontal cortex and motor cortex, pointing out the involvement of brain subnetworks implied in motor behavior, dysfunction of which have been shown in clinical reports(Abboud et al., 2017; Asemi et al., 2015; Walther and Strik, 2012). Lower functional connectivity between the vrPT and sensorimotor cortices was tied to greater severity of both positive and negative-like PLEs; the other areas expressed the opposite pattern, such that increased functional connectivity with vrPT was associate with higher PLE scores. We note however that these LVs did not survive correction for multiple comparisons and require further replication.

Our findings are consistent with a continuum of risk for schizophrenia-like symptoms, in which symptom expression, across a broad spectrum of severity, is related to dorsal CST function. Functional coupling between the DC and dorsolateral PFC was related to the severity of both positive symptom- and negative symptom-like PLEs, suggesting that this neural circuit may be tied to risk for general schizophrenia-like psychopathology.

4.1. Limitations

The majority of participants in our sample (~ 90%) had not yet completed the peak period of risk for schizophrenia at the time of testing. Given that psychotic experiences in early adulthood can predict later psychopathology(Rössler et al., 2007; Werbeloff et al., 2012), some of the subjects analyzed may develop a clinical disorder in a subsequent period. Furthermore, our exclusion of individuals with a history of mental health treatment guaranteed that we were sampling the subclinical range of symptom expression, but it may neglect the more severe end of the PLE spectrum.

Due to our multivariate approach, we cannot draw inferences about single behaviors or voxels, because the optimization in PLS is conducted on the entire data matrix rather than individual behavior and voxels. As such, interpretation of associations between individual variables is restricted to the broader context of the multivariate pattern to which they belong.

Acknowledgments

This work was supported by grants from the National Health and Medical Research Council (ID: 1050504; 1045354), Australian Research Council (ID: FT130100589) and Sylvia and Charles Viertel Foundation. MAB is supported by a Senior Research Fellowship from the Australian National Health and Medical Research Council (NHMRC: 1154378).

Sara Maria Pani gratefully acknowledges Sardinian Regional Government for the financial support of her/his PhD scholarship (P.O.R. Sardegna F.S.E. - Operational Programme of the Autonomous Region of Sardinia, European Social Fund 2014-2020 - Axis III Education and training, Thematic goal 10, Investment Priority 10ii), Specific goal 10.5.

We thank Randy McIntosh (Rotman Research Institute, Toronto - Canada) for his patient advice and Matteo Fraschini (University of Cagliari - Italy) for his continuous support.

Disclosures

The authors declare no competing interests.

Contributors

Alex Fornito and Sara Maria Pani designed the study, Mark Bellgrove, Alex Fornito, and Jeggan Tiego collected the data, Kristina Sabaroedin and Sara Pani processed the data, Sara Maria Pani performed the analysis and drafted the article; all authors provided critical appraisal and final approval of the manuscript.

References

Abboud, R., Noronha, C., Diwadkar, V.A., 2017. Motor system dysfunction in the schizophrenia diathesis: Neural systems to neurotransmitters. Eur. Psychiatry. https://doi.org/10.1016/j.eurpsy.2017.04.004

Anticevic, A., Haut, K., Murray, J.D., Repovs, G., Yang, G.J., Diehl, C., McEwen, S.C., Bearden, C.E., Addington, J., Goodyear, B., Cadenhead, K.S., Mirzakhanian, H., Cornblatt, B.A., Olvet, D., Mathalon, D.H., McGlashan, T.H., Perkins, D.O., Belger, A., Seidman, L.J., Tsuang, M.T., Van Erp, T.G.M., Walker, E.F., Hamann, S., Woods, S.W., Qiu, M., Cannon, T.D., 2015. Association of thalamic dysconnectivity and conversion to psychosis in youth and young adults at elevated clinical risk. JAMA Psychiatry. https://doi.org/10.1001/jamapsychiatry.2015.0566

Asemi, A., Ramaseshan, K., Burgess, A., Diwadkar, V.A., Bressler, S.L., 2015. Dorsal anterior cingulate cortex modulates supplementary motor area in coordinated unimanual motor behavior. Front. Hum. Neurosci. https://doi.org/10.3389/fnhum.2015.00309

Avants, B.B., Tustison, N.J., Song, G., Cook, P.A., Klein, A., Gee, J.C., 2011. A reproducible evaluation of ANTs similarity metric performance in brain image registration. Neuroimage. https://doi.org/10.1016/j.neuroimage.2010.09.025

Cannon, T.D., Van Erp, T.G.M., Glahn, D.C., 2002. Elucidating continuities and discontinuities between schizotypy and schizophrenia in the nervous system, in: Schizophrenia Research. https://doi.org/10.1016/S0920-9964(01)00362-0

Caspi, A., Moffitt, T.E., 2018. All for one and one for all: Mental disorders in one dimension. Am. J. Psychiatry. https://doi.org/10.1176/appi.ajp.2018.17121383

Chapman, L.J., Chapman, J.P., 1980. Scales for rating psychotic and psychotic-like experiences as continua. Schizophr. Bull. https://doi.org/10.1093/schbul/6.3.476

Chapman, L.J., Chapman, J.P., Raulin, M.L., 1978. Body image aberration in schizophrenia. J. Abnorm. Psychol. 87, 399–407. https://doi.org/10.1037//0021-843X.87.4.399

Chapman, L.J., Chapman, J.P., Raulin, M.L., 1976. Scales for physical and social anhedonia. J. Abnorm. Psychol. https://doi.org/10.1037/0021-843X.85.4.374

Dandash, O., Fornito, A., Lee, J., Keefe, R.S.E., Chee, M.W.L., Adcock, R.A., Pantelis, C., Wood, S.J., Harrison, B.J., 2014. Altered striatal functional connectivity in subjects with an at-risk mental state for psychosis. Schizophr. Bull. https://doi.org/10.1093/schbul/sbt093

Dandash, O., Pantelis, C., Fornito, A., 2017. Dopamine, fronto-striato-thalamic circuits and risk for psychosis. Schizophr. Res. https://doi.org/10.1016/j.schres.2016.08.020

Dandash, O., Yücel, M., Daglas, R., Pantelis, C., McGorry, P., Berk, M., Fornito, A., 2018. Differential effect of quetiapine and lithium on functional connectivity of the striatum in first episode mania. Transl. Psychiatry. https://doi.org/10.1038/s41398-018-0108-8

Di Martino, A., Scheres, A., Margulies, D.S., Kelly, A.M.C., Uddin, L.Q., Shehzad, Z., Biswal, B., Walters, J.R., Castellanos, F.X., Milham, M.P., 2008. Functional connectivity of human striatum: A resting state fMRI study. Cereb. Cortex. https://doi.org/10.1093/cercor/bhn041

Draganski, B., Kherif, F., Kloppel, S., Cook, P.A., Alexander, D.C., Parker, G.J.M., Deichmann, R., Ashburner, J., Frackowiak, R.S.J., 2008. Evidence for Segregated and Integrative Connectivity Patterns in the Human Basal Ganglia. J. Neurosci. https://doi.org/10.1523/jneurosci.1486-08.2008

Eckblad, M., Chapman, L.J., 1983. Magical ideation as an indicator of schizotypy. J. Consult. Clin. Psychol. 51, 215–225. https://doi.org/10.1037/0022-006X.51.2.215

efron, B Tibshirani, R., 1986. boostratp methods for standard errors, confidence intervals, and other masures of statistical accuracy. Stat. Rev.

Ettinger, U., Meyhöfer, I., Steffens, M., Wagner, M., Koutsouleris, N., 2014. Genetics, cognition, and neurobiology of schizotypal personality: A review of the overlap with schizophrenia. Front. Psychiatry. https://doi.org/10.3389/fpsyt.2014.00018

Ettinger, U., Williams, S.C.R., Meisenzahl, E.M., Möller, H.J., Kumari, V., Koutsouleris, N., 2012.

Association between brain structure and psychometric schizotypy in healthy individuals. World J. Biol. Psychiatry. https://doi.org/10.3109/15622975.2011.559269

Fonseca-Pedrero, E., Ortuño-Sierra, J., Mason, O.J., Muñiz, J., 2015. The Oxford-Liverpool Inventory of Feelings and Experiences short version: Further validation. Pers. Individ. Dif. https://doi.org/10.1016/j.paid.2015.06.041

Fornito, A., Harrison, B.J., Goodby, E., Dean, A., Ooi, C., Nathan, P.J., Lennox, B.R., Jones, P.B., Suckling, J., Bullmore, E.T., 2013. Functional dysconnectivity of corticostriatal circuitry as a risk phenotype for psychosis. JAMA Psychiatry. https://doi.org/10.1001/jamapsychiatry.2013.1976

Fornito, A., Radua, J., Walterfang, M., Seal, M., Wood, S.J., Yucel, M., Velakoulis, D., Pantelis, C., 2011. Neuroanatomical abnormalities in schizophrenia: a multimodal voxelwise meta-analysis and meta-regression analysis. Schizophr. Res.

Fornito, A., Yücel, M., Wood, S.J., Adamson, C., Velakoulis, D., Saling, M.M., McGorry, P.D., Pantelis, C., 2008. Surface-based morphometry of the anterior cingulate cortex in first episode schizophrenia. Hum. Brain Mapp. https://doi.org/10.1002/hbm.20412

Garrity, A.G., Pearlson, G.D., McKiernan, K., Lloyd, D., Kiehl, K.A., Calhoun, V.D., 2007. Aberrant "default mode" functional connectivity in schizophrenia. Am. J. Psychiatry. https://doi.org/10.1176/ajp.2007.164.3.450

Grace, A.A., 2016. Dysregulation of the dopamine system in the pathophysiology of schizophrenia and depression. Nat. Rev. Neurosci. https://doi.org/10.1038/nrn.2016.57

Grant, P., Green, M.J., Mason, O.J., 2018. Models of Schizotypy: The Importance of Conceptual Clarity. Schizophr. Bull. https://doi.org/10.1093/schbul/sby012

Griffanti, L., Salimi-Khorshidi, G., Beckmann, C.F., Auerbach, E.J., Douaud, G., Sexton, C.E., Zsoldos, E., Ebmeier, K.P., Filippini, N., Mackay, C.E., Moeller, S., Xu, J., Yacoub, E., Baselli, G., Ugurbil, K., Miller, K.L., Smith, S.M., 2014. ICA-based artefact removal and accelerated fMRI acquisition for improved resting state network imaging. Neuroimage.

https://doi.org/10.1016/j.neuroimage.2014.03.034

Haber, S.N., 2016. Corticostriatal circuitry, in: Neuroscience in the 21st Century: From Basic to Clinical, Second Edition. https://doi.org/10.1007/978-1-4939-3474-4_135

Haber, S.N., Knutson, B., 2010. The reward circuit: Linking primate anatomy and human imaging. Neuropsychopharmacology. https://doi.org/10.1038/npp.2009.129

Howes, O.D., Montgomery, A.J., Asselin, M.C., Murray, R.M., Valli, I., Tabraham, P., Bramon-Bosch, E., Valmaggia, L., Johns, L., Broome, M., McGuire, P.K., Grasby, P.M., 2009. Elevated striatal dopamine function linked to prodromal signs of schizophenia. Arch. Gen. Psychiatry. https://doi.org/10.1001/archgenpsychiatry.2008.514

Huttunen, J., Heinimaa, M., Svirskis, T., Nyman, M., Kajander, J., Forsback, S., Solin, O., Ilonen, T., Korkeila, J., Ristkari, T., McGlashan, T., Salokangas, R.K.R., Hietala, J., 2008. Striatal Dopamine Synthesis in First-degree Relatives of Patients with Schizophrenia. Biol. Psychiatry. https://doi.org/10.1016/j.biopsych.2007.04.017

Jacobson, S., Kelleher, I., Harley, M., Murtagh, A., Clarke, M., Blanchard, M., Connolly, C., O'Hanlon, E., Garavan, H., Cannon, M., 2010. Structural and functional brain correlates of subclinical psychotic symptoms in 11-13 year old schoolchildren. Neuroimage. https://doi.org/10.1016/j.neuroimage.2009.09.015

Kelleher, I., Cannon, M., 2011. Psychotic-like experiences in the general population: Characterizing a high-risk group for psychosis. Psychol. Med. https://doi.org/10.1017/S0033291710001005

Krishnan, A., Williams, L.J., McIntosh, A.R., Abdi, H., 2011. Partial Least Squares (PLS) methods for neuroimaging: A tutorial and review. Neuroimage. https://doi.org/10.1016/j.neuroimage.2010.07.034

Lee, S.H., Decandia, T.R., Ripke, S., Yang, J., Sullivan, P.F., Goddard, M.E., Keller, M.C., Visscher, P.M., Wray, N.R., 2012. Estimating the proportion of variation in susceptibility to schizophrenia captured by common SNPs. Nat. Genet. https://doi.org/10.1038/ng.1108

McIntosh, A.R., Bookstein, F.L., Haxby, J. V., Grady, C.L., 1996. Spatial pattern analysis of functional brain images using partial least squares. Neuroimage. https://doi.org/10.1006/nimg.1996.0016

Mossaheb, N., Becker, J., Schaefer, M.R., Klier, C.M., Schloegelhofer, M., Papageorgiou, K., Amminger, G.P., 2012. The Community Assessment of Psychic Experience (CAPE) questionnaire as a screening-instrument in the detection of individuals at ultra-high risk for psychosis. Schizophr. Res. https://doi.org/10.1016/j.schres.2012.08.008

Parkes, L., Fulcher, B., Yücel, M., Fornito, A., 2018. An evaluation of the efficacy, reliability, and sensitivity of motion correction strategies for resting-state functional MRI. Neuroimage. https://doi.org/10.1016/j.neuroimage.2017.12.073

Peters, E., Joseph, S., Day, S., Garety, P., 2004. Measuring delusional ideation: the 21-Item Peters et al. Delusions Inventory. Schizophr. Bull. 30, 1005–1022. https://doi.org/10.1037/t03329-000

R., P., A., C., T.E., M., M., C., R., M., Poulton, R., Caspi, A., Moffitt, T.E., Cannon, M., Murray, R., Harrington, H., 2000. Children's self-reported psychotic symptoms and adult schizophreniform disorder: a 15-year longitudinal study. Arch. Gen. Psychiatry.

Reid, M.A., Stoeckel, L.E., White, D.M., Avsar, K.B., Bolding, M.S., Akella, N.S., Knowlton, R.C., Den Hollander, J.A., Lahti, A.C., 2010. Assessments of function and biochemistry of the anterior cingulate cortex in schizophrenia. Biol. Psychiatry. https://doi.org/10.1016/j.biopsych.2010.04.013

Rössler, W., Riecher-Rössler, A., Angst, J., Murray, R., Gamma, A., Eich, D., van Os, J., Gross, V.A., 2007. Psychotic experiences in the general population: A twenty-year prospective community study. Schizophr. Res. https://doi.org/10.1016/j.schres.2007.01.002

Sabaroedin, K., Tiego, J., Parkes, L., Sforazzini, F., Finlay, A., Johnson, B., Pinar, A., Cropley, V., Harrison, B.J., Zalesky, A., Pantelis, C., Bellgrove, M., Fornito, A., 2019. Functional Connectivity of Corticostriatal Circuitry and Psychosis-Like Experiences in the General Community. Biol. Psychiatry. https://doi.org/10.1016/j.biopsych.2019.02.013

Salimi-Khorshidi, G., Douaud, G., Beckmann, C.F., Glasser, M.F., Griffanti, L., Smith, S.M., 2014.

Automatic denoising of functional MRI data: Combining independent component analysis and hierarchical fusion of classifiers. Neuroimage. https://doi.org/10.1016/j.neuroimage.2013.11.046

Satterthwaite, T.D., Vandekar, S.N., Wolf, D.H., Bassett, D.S., Ruparel, K., Shehzad, Z., Craddock, R.C., Shinohara, R.T., Moore, T.M., Gennatas, E.D., Jackson, C., Roalf, D.R., Milham, M.P., Calkins, M.E., Hakonarson, H., Gur, R.C., Gur, R.E., 2015. Connectome-wide network analysis of youth with Psychosis-Spectrum symptoms. Mol. Psychiatry. https://doi.org/10.1038/mp.2015.66

Sheffield, J.M., Kandala, S., Burgess, G.C., Harms, M.P., Barch, D.M., 2016. Cingulo-opercular Network Efficiency Mediates the Association Between Psychotic-like Experiences and Cognitive Ability in the General Population. Biol. Psychiatry Cogn. Neurosci. Neuroimaging. https://doi.org/10.1016/j.bpsc.2016.03.009

Simpson, E.H., Kellendonk, C., Kandel, E., 2010. A Possible Role for the Striatum in the Pathogenesis of the Cognitive Symptoms of Schizophrenia. Neuron. https://doi.org/10.1016/j.neuron.2010.02.014

Skudlarski, P., Schretlen, D.J., Thaker, G.K., Stevens, M.C., Keshavan, M.S., Sweeney, J.A., Tamminga, C.A., Clementz, B.A., O'Neil, K., Pearlson, G.D., 2013. Diffusion tensor imaging white matter endophenotypes in patients with schizophrenia or psychotic bipolar disorder and their relatives. Am. J. Psychiatry. https://doi.org/10.1176/appi.ajp.2013.12111448

Stefanis, N.C., Hanssen, M., Smirnis, N.K., Avramopoulos, D.A., Evdokimidis, I.K., Stefanis, C.N., Verdoux, H., Van Os, J., 2002. Evidence that three dimensions of psychosis have a distribution in the general population. Psychol. Med. https://doi.org/10.1017/S0033291701005141

Study, A. frontostriatal interactions in people with prodromal signs of psychosis: A. multimodal imaging, 2010. Abnormal frontostriatal interactions in people with prodromal signs of psychosis: A multimodal imaging study. Arch. Gen. Psychiatry. https://doi.org/10.1001/archgenpsychiatry.2010.77

Tandon, N., Montrose, D., Shah, J., Rajarethinam, R.P., Diwadkar, V.A., Keshavan, M.S., 2012. Early prodromal symptoms can predict future psychosis in familial high-risk youth. J. Psychiatr. Res. https://doi.org/10.1016/j.jpsychires.2011.09.019

Unterrassner, L., Wyss, T.A., Wotruba, D., Ajdacic-Gross, V., Haker, H., Rössler, W., 2017. Psychotic-like experiences at the healthy end of the psychosis continuum. Front. Psychol. https://doi.org/10.3389/fpsyg.2017.00775

Van Os, J., Linscott, R.J., Myin-Germeys, I., Delespaul, P., Krabbendam, L., 2009. A systematic review and meta-analysis of the psychosis continuum: Evidence for a psychosis proneness-persistence-impairment model of psychotic disorder. Psychol. Med. https://doi.org/10.1017/S0033291708003814

van Os, J., Verdoux, H., Maurice-Tison, S., Gay, B., Liraud, F., Salamon, R., Bourgeois, M., 1999. Self-reported psychosis-like symptoms and the continuum of psychosis. Soc. Psychiatry Psychiatr. Epidemiol.

Verdoux, H., van Os, J., 2002. Psychotic symptoms in non-clinical populations and the continuum of psychosis. Schizophr. Res.

Walther, S., Strik, W., 2012. Motor symptoms and schizophrenia. Neuropsychobiology. https://doi.org/10.1159/000339456

Werbeloff, N., Drukker, M., Dohrenwend, B.P., Levav, I., Yoffe, R., Van Os, J., Davidson, M., Weiser, M., 2012. Self-reported attenuated psychotic symptoms as forerunners of severe mental disorders later in life. Arch. Gen. Psychiatry. https://doi.org/10.1001/archgenpsychiatry.2011.1580

White, T.P., Joseph, V., Francis, S.T., Liddle, P.F., 2010. Aberrant salience network (bilateral insula and anterior cingulate cortex) connectivity during information processing in schizophrenia. Schizophr. Res. https://doi.org/10.1016/j.schres.2010.07.020

Woodward, N.D., Heckers, S., 2016. Mapping Thalamocortical Functional Connectivity in Chronic and Early Stages of Psychotic Disorders. Biol. Psychiatry. https://doi.org/10.1016/j.biopsych.2015.06.026

Woolrich, M.W., Ripley, B.D., Brady, M., Smith, S.M., 2001. Temporal autocorrelation in univariate linear modeling of FMRI data. Neuroimage. https://doi.org/10.1006/nimg.2001.0931

LEGENDS FOR TABLES AND FIGURES

Table1. PLE subscales list and descriptive statistic (*n*=353). CAPE: Community assessment of psychotic experiences; Chapman Scales; sO-LIFE: Oxford-Liverpool inventory of feelings and experiences short form; PDI: Peters delusion inventory.

Figure 1. **Association between dorsal caudate functional connectivity and PLEs: LV1.** A: Correlations between each PLE subscale, age, sex, and brain scores for LV1 in the PLS of dorsal caudate functional connectivity. Error bars represent 95% confidence intervals. The intervals do not cross zero for any PLEs scale; therefore, this LV contains significant loadings from all PLEs measures. Blue: left DC seed-related FC; Red: right DC seed-related FC. B: Axial slices through the bootstrap image showing regions reliably contributing to LV1. Cool colors identify regions where DC-related functional connectivity was associated with the multivariate profile depicted in panel A (i.e., higher functional connectivity was associated with lower scores); warm colors show the opposite. Left hemisphere is on the left. CAPE: community assessment of psychotic experience; sO-LIFE: Oxford-Liverpool Inventory of feelings and experiences short-form. PDI: Peters delusion inventory.

Figure 2. Spatial consistency of dorsal corticostriatal circuit involvement across a broad spectrum of psychosis severity. The coronal slice on the left shows the location of the dorsal caudate (DC) seed region. The cortical surface map on the right depicts the area of dorsolateral prefrontal cortex where seed-related functional connectivity correlates with PLE severity in our community sample, together with prefrontal areas implicated in past work conducted in patients with first-episode psychosis and their first-degree relatives (Fornito, JAMA Psych), ARMS individuals (Dandash), first episode mania patients with psychosis (Dandash). The map of positive symptoms maps regions associated with positive symptom severity in first episode psychosis patients (Fornito JAMA Psych).

TABLES

Table 1

PLEs Subscales	Mean	SD
CAPE		
1. Positive	25.72	4.72
2. Negative	23.99	5.84
3. Depressive	13.84	2.97
Chapman		
4. Magical Ideation	6.11	4.61
5. Physical Anhedonia	11.81	7.19
6. Perceptual Aberration	5.12	5.17
7. Revised Social Anhedonia	9.64	6.78
sO-LIFE		
8. Unusual Experiences	2.89	2.65
9. Cognitive Disorganization	4.67	2.92
10. Introvertive Anhedonia	1.69	1.8
11. Impulsive Non-conformity	3.18	2.1
12. PDI Total Score	5.32	3.44
AGE	**Mean**	**SD**
	23.4	5.16
SEX	**F**	**M**
	198	155

FIG.1

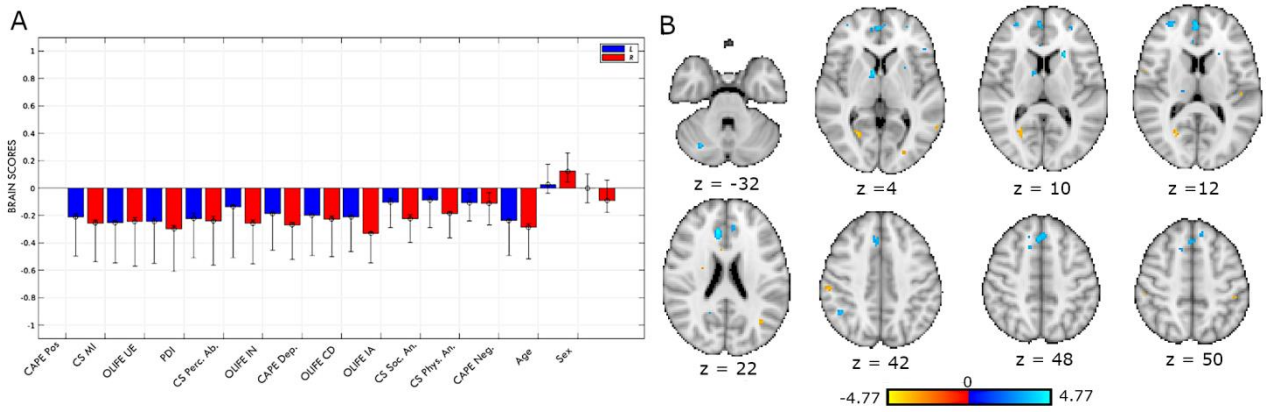
A
BRAIN SCORES
CAPE Pos.
CS MI
OLIFE UE
PDI
CS Perc. Ab.
OLIFE IN
CAPE Dep.
OLIFE CD
OLIFE IA
CS Soc. An.
CS Phys. An.
CAPE Neg.
Age
Sex
B
z = -32
z =4
z = 10
z =12
z = 22
z = 42
z = 48
z = 50
-4.77
0
4.77

FIG.2

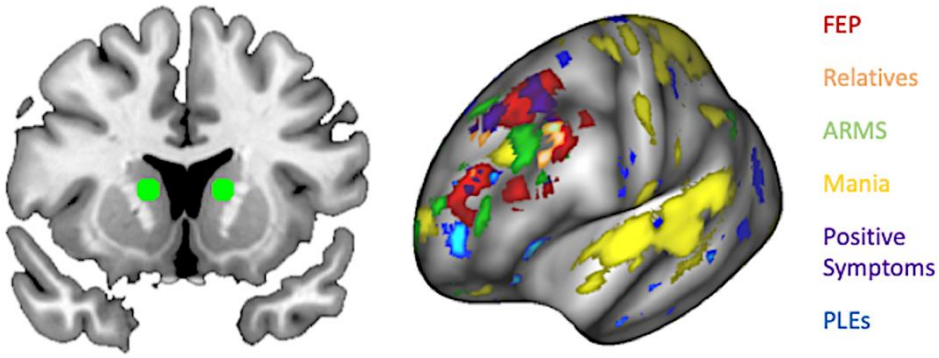
FEP
Relatives
ARMS
Mania
Positive Symptoms
PLEs

SUPPLEMENTAL INFORMATION

Supplementary Figures and Tables DC-Related Analysis

SF1. Percent crossblock covariance plot, DC related analysis.

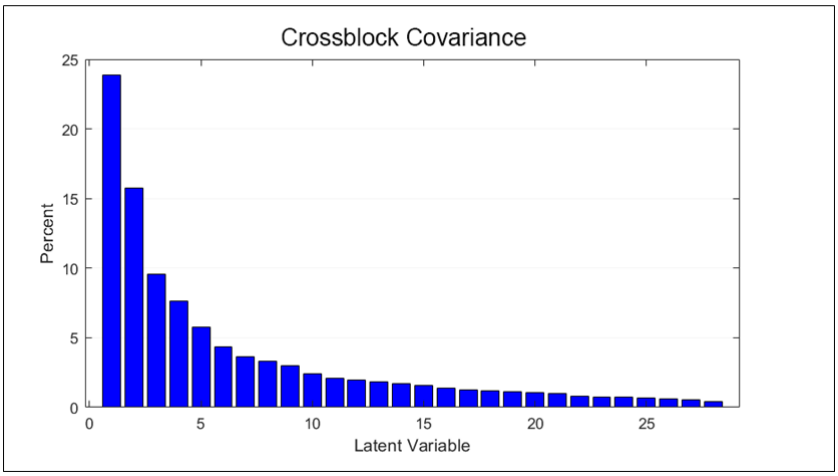

SF2. **Brain scores vs behavioural measures. Dc-related analysis, LV1**: brain scores are plotted against behavioural measures for each condition respectively. Behavioural scores shown CAPE (Community assessment of psychotic experiences) negative and positive.

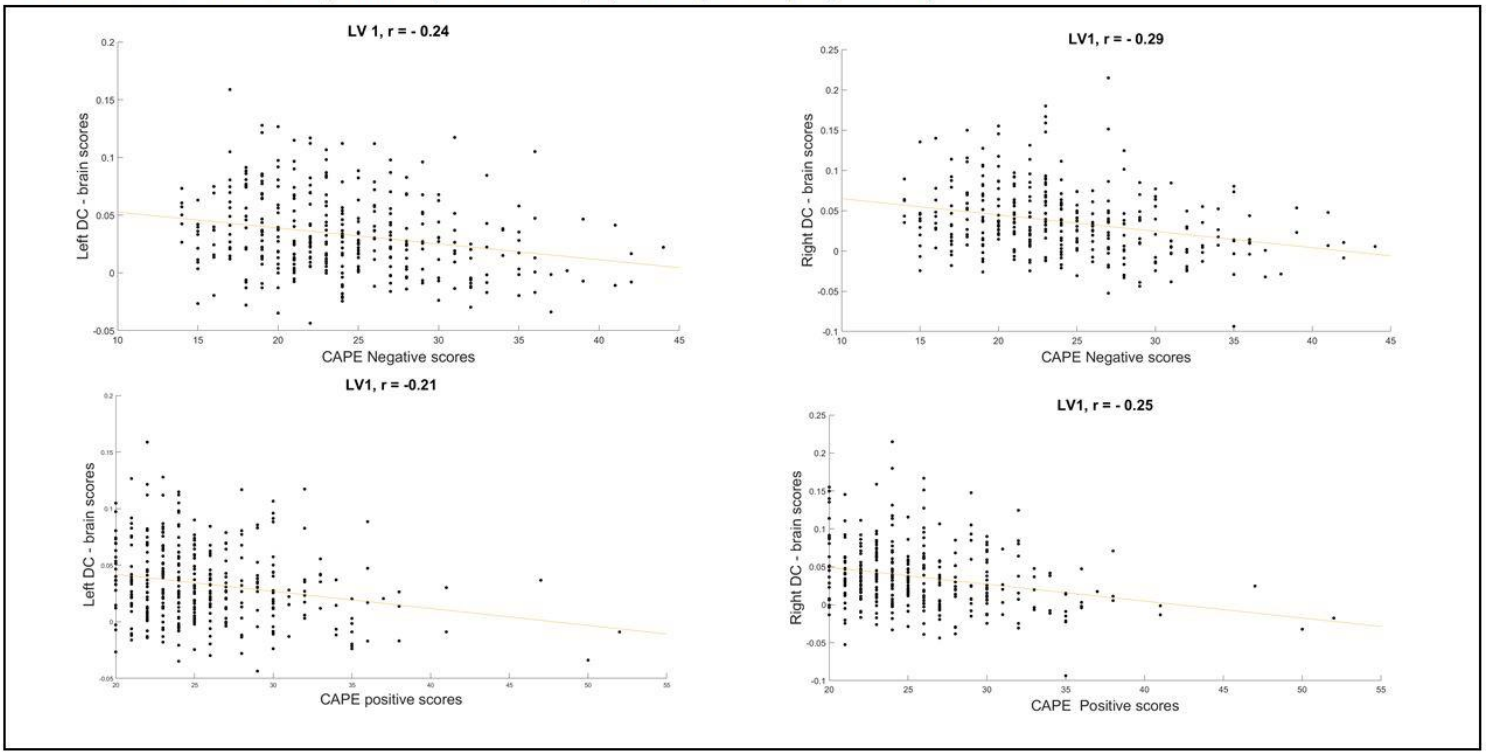

**ST1 Cluster sizes and peak coordinates for bootstrap image of LV1, DC analysis. ***Voxel mean: the average for all voxels in the cluster that passed the bootstrap ratio threshold.

		Peak Location						Bootstrap		Cluster size
Cluster#	*Voxel Mean	X	Y	Z	X(mm)	Y(mm)	Z(mm)	BSR	Appro.P	(voxels)
1	0.00023842245	41	81	48	-10.0	34.0	22.0	47.179	0.0000	93
2	0.0013775049	42	65	40	-8.0	2.0	6.0	43.940	0.0000	38
3	0.00024050951	31	29	22	-30.0	-70.0	-30.0	43.893	0.0000	19
4	0.00019230139	57	75	42	22.0	22.0	10.0	42.891	0.0000	12
5	0.00010601819	24	39	57	-44.0	-50.0	40.0	41.786	0.0000	19
6	0.000078363722	60	89	41	28.0	50.0	8.0	40.703	0.0000	13
7	0.00035506504	44	77	61	-4.0	26.0	48.0	39.394	0.0001	81
8	0.000018105024	37	37	49	-18.0	-54.0	24.0	39.159	0.0001	5
9	0.00030679931	45	89	43	-2.0	50.0	12.0	39.008	0.0001	77
10	0.00016977615	42	84	52	-8.0	40.0	30.0	38.717	0.0001	15
11	0.00011267293	49	38	12	6.0	-52.0	-50.0	38.072	0.0001	14
12	0.00020766587	50	83	47	8.0	38.0	20.0	37.481	0.0002	24
13	0.00015451499	70	78	38	48.0	28.0	2.0	37.431	0.0002	18
14	0.000051767773	32	40	44	-28.0	-48.0	14.0	37.367	0.0002	6
15	-0.000065115237	30	28	54	-32.0	-72.0	34.0	36.703	0.0002	8
16	0.00015179534	51	81	62	10.0	34.0	50.0	36.627	0.0002	5
17	0.00003472915	39	73	60	-14.0	18.0	46.0	36.030	0.0003	11
18	0.00021661719	31	90	43	-30.0	52.0	12.0	35.755	0.0003	23
19	0.00020473395	50	39	17	8.0	-50.0	-40.0	34.335	0.0006	5
20	0.00023416663	69	78	33	46.0	28.0	-8.0	34.194	0.0006	9
21	0.00017387600	49	85	53	6.0	42.0	32.0	33.829	0.0007	10
22	-0.000089600266	34	31	44	-24.0	-66.0	14.0	-41.890	0.0000	64
23	-0.00031887120	50	33	35	8.0	-62.0	-4.0	-37.943	0.0001	9
24	-0.000047167487	27	66	36	-38.0	4.0	-2.0	-36.828	0.0002	10
25	-0.00031904009	17	51	60	-58.0	-26.0	46.0	-36.628	0.0002	25
26	-0.00011567139	45	64	54	-2.0	0.0	34.0	-36.400	0.0003	7
27	-0.00015012096	66	32	46	40.0	-64.0	18.0	-36.336	0.0003	25
28	-0.00010147665	39	41	40	-14.0	-46.0	6.0	-35.746	0.0004	10
29	0.000074216696	27	66	50	-38.0	4.0	26.0	-35.687	0.0004	6
30	-0.00009242841	58	22	37	24.0	-84.0	0.0	-33.130	0.0009	10
31	-0.00018245907	68	46	64	44.0	-36.0	54.0	-33.023	0.0010	9
32	-0.00017386273	76	38	41	60.0	-52.0	8.0	-32.804	0.0010	7
33	-0.00024608569	35	31	65	-22.0	-66.0	56.0	-32.501	0.0012	5

Supplementary Figures and Tables Associations Significant at Uncorrected Levels

SF3. Percent Crossblock Covariance plot, dcPT related analysis.

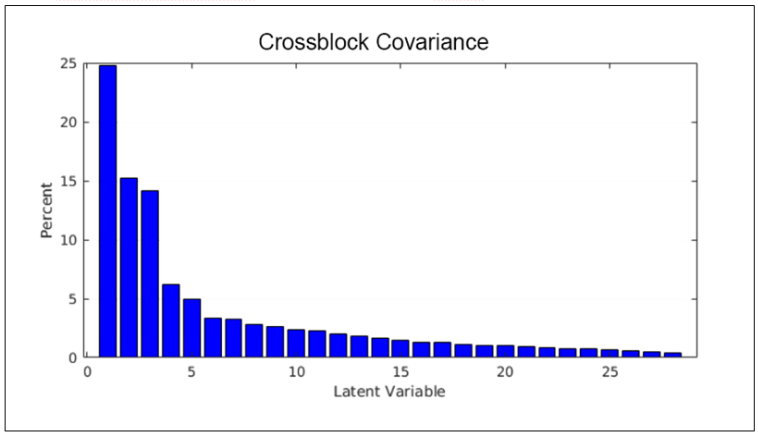

SF4. Associations between dorsocaudal putamen functional connectivity and PLEs: LV1.

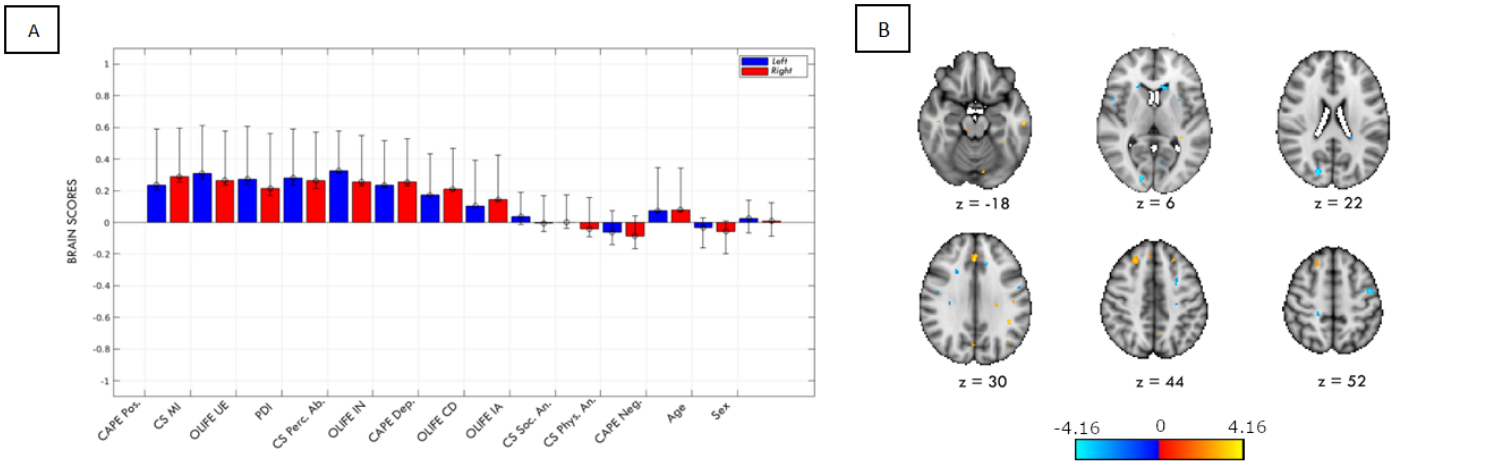

A:Correlations between each PLE scale, age, and sex and brain scores for LV1 in the PLS of dorsocaudal putamen(DCP)functional connectivity (FC). Error bars represent 95% confidence intervals. LV1 doesn't contains significant loadings from the PLE measures whose intervals cross zero. Blue: left DCP seed-related FC: Red: right DCP see-related FC. B: Axial slices through the bootstrap image showing regions reliably contributing to LV1. Warm colours identify regions where DCP-related functional connectivity was associated with the multivariate profile depicted in panel A (i.e., higher functional connectivity was associated with higher scores); cool colours show the opposite. Left hemisphere is on the left.
CAPE: community assessment of psychotic experience; sO-LIFE: Oxford-Liverpool Inventory of feelings and experiences short-form. PDI: Peters delusion inventory.

SF5. Associations between dorsocaudal putamen functional connectivity and PLEs: LV2.

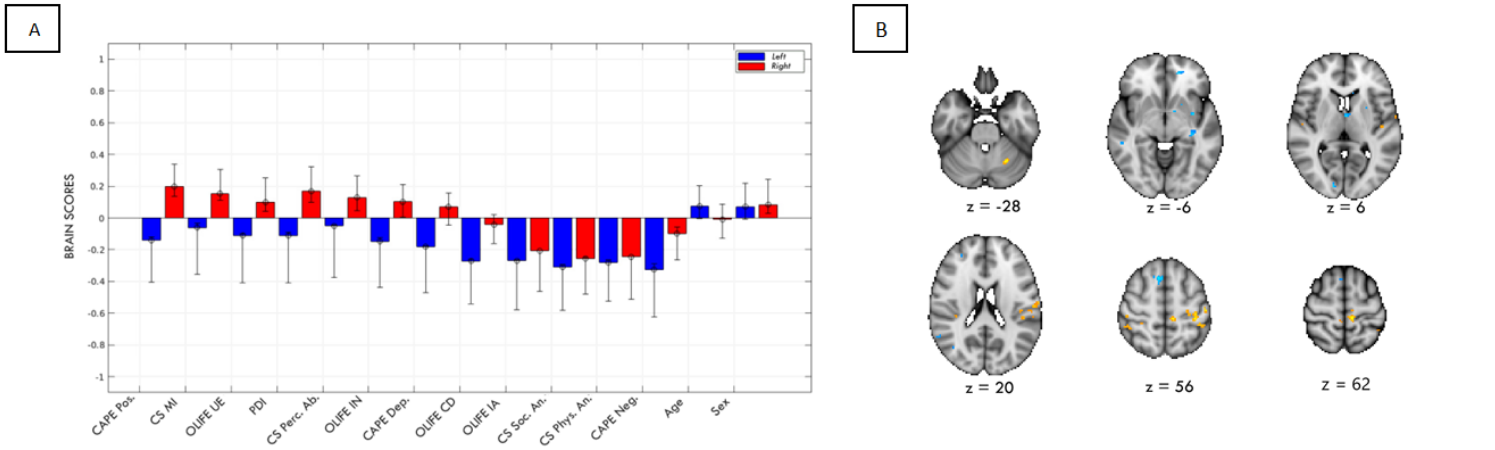

A: Correlations between each PLE scale, age, and sex and brain scores for LV1 in the PLS of dorsocaudal putamen(DCP)functional connectivity (FC). Error bars represent 95% confidence intervals. LV1 doesn't contains significant loadings from the PLE measures whose intervals cross zero. Blue: left DCP seed-related FC: Red: right DCP seed-related FC. B: Axial slices through the bootstrap image showing regions reliably contributing to LV1. Cool colours identify regions where DCP-related functional connectivity was associated with the multivariate profile depicted in panel A (i.e., higher functional connectivity was associated with lower scores); warm colours show the opposite. Left hemisphere is on the left.
CAPE: community assessment of psychotic experience; sO-LIFE: Oxford-Liverpool Inventory of feelings and experiences short-form. PDI: Peters delusion inventory.

ST2 Cluster sizes and peak coordinates for bootstrap image of LV1, DCP analysis. Voxel mean: the average for all voxels in the cluster that passed the bootstrap ratio threshold.

		Peak Location						Bootstrap		Cluster Size
Cluster#	Voxel Mean	X	Y	Z	X(mm)	Y(mm)	Z(mm)	BSR	Appro.P	(voxels)
1	-0.00010197205	58	49	36	24.0	-30.0	-2.0	41.586	0.0000	10
2	0.000026737247	33	42	19	-26.0	-44.0	-36.0	41.163	0.0000	22
3	0.000037651153	45	80	52	-2.0	32.0	30.0	40.121	0.0001	51
4	-0.00012873425	76	54	28	60.0	-20.0	-18.0	39.571	0.0001	11
5	- 0,000042118885	53	24	26	14.0	-80.0	-22.0	39.511	0.0001	17
6	- 0.000028518742	67	42	52	42.0	-44.0	30.0	39.374	0.0001	15
7	- 0.00001817798	60	53	50	28.0	-22.0	26.0	39.301	0.0001	11
8	0.000029709641	59	71	29	26.0	14.0	-16.0	38.812	0.0001	12
9	0.00012799514	62	74	35	32.0	20.0	-4.0	38.655	0.0001	34
10	- 0.000016764996	60	44	42	28.0	-40.0	10.0	37.139	0.0002	11
11	-0.00017481492	35	79	59	-22.0	30.0	44.0	36.665	0.0002	71
12	0.00013271977	28	71	33	-36.0	14.0	-8.0	36.519	0.0003	9
13	- 0.000052796753	44	85	43	-4.0	42.0	12.0	35.850	0.0003	16
14	- 0.0000543,6199	32	23	20	-28.0	-82.0	-34.0	35.598	0.0004	9
15	0.00011224924	47	59	55	2.0	-10.0	36.0	35.479	0.0004	5
16	-0.00047098071	45	28	54	-2.0	-72.0	34.0	35.305	0.0004	22
17	-0.00014677091	45	88	36	-2.0	48.0	-2.0	34.421	0.0006	6
18	- 0.0000220,18283	42	84	55	-8.0	40.0	36.0	34.120	0.0006	14
19	- 0.000039728322	39	51	31	-14.0	-26.0	-12.0	33.837	0.0007	5
20	-0.00016577356	61	73	62	30.0	18.0	50.0	33.773	0.0007	6
21	-0.00024706137	73	38	54	54.0	-52.0	34.0	33.653	0.0008	11
22	-0.00010000667	43	82	60	-6.0	36.0	46.0	33.392	0.0008	7
23	-0.00018131082	58	80	59	24.0	32.0	44.0	32.884	0.0010	6
24	-0.00029252379	46	46	56	0.0	-36.0	38.0	32.623	0.0011	12
25	-0.00014402569	65	30	54	38.0	-68.0	34.0	32.384	0.0012	6
26	- 0.000026932903	37	24	48	-18.0	-80.0	22.0	-47.164	0.0000	52
27	- 0.000062691361	38	20	40	-16.0	-88.0	6.0	-44.210	0.0000	25
28	0.00015426076	68	61	62	44.0	-6.0	50.0	-43.345	0.0000	48
29	- 0.0000019973497	56	80	43	20.0	32.0	12.0	-42.042	0.0000	34
30	- 0.000024606401	54	82	34	16.0	36.0	-6.0	-40.559	0.0000	17
31	- 0.000051780073	51	76	40	10.0	24.0	6.0	-39.240	0.0001	20
32	- 0.000074133481	39	34	32	-14.0	-60.0	-10.0	-39.141	0.0001	20
33	0.000041622159	53	77	52	14.0	26.0	30.0	-38.705	0.0001	6
34	0.00014337248	32	60	45	-28.0	-8.0	16.0	-37.756	0.0002	7
35	0.0010221736	58	60	37	24.0	-8.0	0.0	-37.047	0.0002	15
36	0.00003913078	36	76	39	-20.0	24.0	4.0	-36.817	0.0002	11
37	- 0.000016015616	59	66	59	26.0	4.0	44.0	-36.797	0.0002	14
38	0.000022248805	38	46	62	-16.0	-36.0	50.0	-36.690	0.0002	21
39	0.00016867838	56	57	74	20.0	-14.0	74.0	-36.676	0.0002	11
40	0.000030528383	29	79	44	-34.0	30.0	14.0	-36.317	0.0003	11
41	0.00043335190	44	62	72	-4.0	-4.0	70.0	-35.915	0.0003	9

42	- 0.000035606463	30	75	53	-32.0	22.0	32.0	-35.506	0.0004	20
43	- 0.000025643993	30	26	31	-32.0	-76.0	-12.0	-35.460	0.0004	11
44	0.00049699657	48	64	68	4.0	0.0	62.0	-35.394	0.0004	25
45	0.00043413648	36	61	37	-20.0	-6.0	0.0	-35.380	0.0004	5
46	-0.00014236677	57	44	34	22.0	-40.0	-6.0	-35.120	0.0004	9
47	0.000054361553	23	61	52	-46.0	-6.0	30.0	-34.566	0.0005	12
48	0.00064334739	61	56	38	30.0	-16.0	2.0	-34.469	0.0006	6
49	- 0.000016628441	30	55	50	-32.0	-18.0	26.0	-34.445	0.0006	6
50	0.00018945022	21	69	42	-50.0	10.0	10.0	-34.383	0.0006	12
51	0.00013542535	73	64	52	54.0	0.0	30.0	-33.416	0.0008	6
52	-0.00024333075	49	29	39	6.0	-70.0	4.0	-32.630	0.0011	7

ST3 Cluster sizes and peak coordinates for bootstrap image of LV2, DCP analysis. Voxel mean: the average for all voxels in the cluster that passed the bootstrap ratio threshold.

		Peak Location						Bootstrap		Cluster Size
Cluster#	Voxel Mean	X	Y	Z	X(mm)	Y(mm)	Z(mm)	BSR	Appro.P	(voxels)
1	0.000010812002	44	73	64	-4.0	18.0	54.0	42.549	0.0000	42
2	- 0.000037576028	48	39	19	4.0	-50.0	-36.0	40.992	0.0000	22
3	0.000076989825	51	65	35	10.0	2.0	-4.0	40.122	0.0001	26
4	0.000083642874	29	61	25	-34.0	-6.0	-24.0	39.341	0.0001	17
5	- 0.000020315198	54	88	34	16.0	48.0	-6.0	39.315	0.0001	31
6	0.0012646960	63	63	34	34.0	-2.0	-6.0	39.076	0.0001	8
7	- 0.000029380226	61	60	51	30.0	-8.0	28.0	38.592	0.0001	18
8	- 0.000080634796	39	19	40	-14.0	-90.0	6.0	37.392	0.0002	9
9	-0.00022546921	26	30	52	-40.0	-68.0	30.0	37.344	0.0002	20
10	-0.00012326667	74	40	51	56.0	-48.0	28.0	36.579	0.0003	19
11	- 0.000030241692	62	51	34	32.0	-26.0	-6.0	35.998	0.0003	18
12	-0.00041300416	46	43	49	0.0	-42.0	24.0	35.710	0.0004	6
13	0.00022618833	43	64	38	-6.0	0.0	2.0	35.427	0.0004	10
14	0.000058994847	47	80	44	2.0	32.0	14.0	35.156	0.0004	15
15	-0.00020008520	19	45	34	-54.0	-38.0	-6.0	34.693	0.0005	7
16	0.00002598122	51	76	37	10.0	24.0	0.0	34.622	0.0005	5
17	0.00021467764	31	86	48	-30.0	44.0	22.0	34.603	0.0005	21
18	0.00001903974	57	76	31	22.0	24.0	-12.0	33.516	0.0008	5
19	- 0.000023544129	62	44	54	32.0	-40.0	34.0	33.513	0.0008	6
20	0.00026764924	44	65	70	-4.0	2.0	66.0	33.064	0.0009	5
21	-0.00021852728	53	16	36	14.0	-96.0	-2.0	32.772	0.0010	7
22	-0.00018992936	18	37	48	-56.0	-54.0	22.0	32.613	0.0011	8
23	0.00010913133	58	34	24	24.0	-60.0	-26.0	-44.802	0.0000	29
24	0.000023188539	51	48	66	10.0	-32.0	58.0	-43.533	0.0000	71
25	0.00017432158	49	55	63	6.0	-18.0	52.0	-43.231	0.0000	20

26	0.00017366311	60	57	45	28.0	-14.0	16.0	-42.518	0.0000	14
27	- 0.000044297285	74	54	62	56.0	-20.0	50.0	-41.624	0.0000	95
28	- 0.000023951821	64	48	65	36.0	-32.0	56.0	-41.588	0.0000	99
29	- 0.000055253051	68	43	67	44.0	-42.0	60.0	-39.875	0.0001	63
30	0.00015896579	19	66	51	-54.0	4.0	28.0	-39.673	0.0001	10
31	0.000012101009	31	45	62	-30.0	-38.0	50.0	-39.643	0.0001	16
32	0.00021746341	54	59	74	16.0	-10.0	74.0	-39.124	0.0001	10
33	0.00013108287	51	53	36	10.0	-22.0	-2.0	-38.097	0.0001	9
34	0.000073203366	15	54	55	-62.0	-20.0	36.0	-37.661	0.0002	7
35	0.000067206383	53	52	70	14.0	-24.0	66.0	-37.131	0.0002	13
36	0.0000526808	57	60	29	22.0	-8.0	-16.0	-37.006	0.0002	14
37	0.00018311058	28	50	45	-36.0	-28.0	16.0	-36.597	0.0003	19
38	0.00016910824	78	58	47	64.0	-12.0	20.0	-36.407	0.0003	55
39	0.00010438367	68	53	46	44.0	-22.0	18.0	-35.993	0.0003	20
40	- 0.000093479124	55	28	36	18.0	-72.0	-2.0	-35.624	0.0004	6
41	0.00021631589	26	60	38	-40.0	-8.0	2.0	-35.166	0.0004	6
42	- 0.000037073118	47	48	71	2.0	-32.0	68.0	-34.811	0.0005	10
43	0.00030485971	74	65	36	56.0	2.0	-2.0	-34.510	0.0006	5
44	- 0.00009786756	22	50	63	-48.0	-28.0	52.0	-34.316	0.0006	20
45	- 0.00000044421199	68	52	57	44.0	-24.0	40.0	-34.157	0.0006	10
46	0.00029776222	41	63	57	-10.0	-2.0	40.0	-34.024	0.0007	9
47	0.00037411274	66	64	42	40.0	0.0	10.0	-33.620	0.0008	6
48	0.00004302707	39	52	37	-14.0	-24.0	0.0	-33.287	0.0009	10
49	- 0.000046294728	33	28	36	-26.0	-72.0	-2.0	-32.823	0.0010	7
50	-0.00012342352	24	43	65	-44.0	-42.0	56.0	-32.768	0.0010	10

SF6. Percent Crossblock Covariance plot, vrPT related analysis.

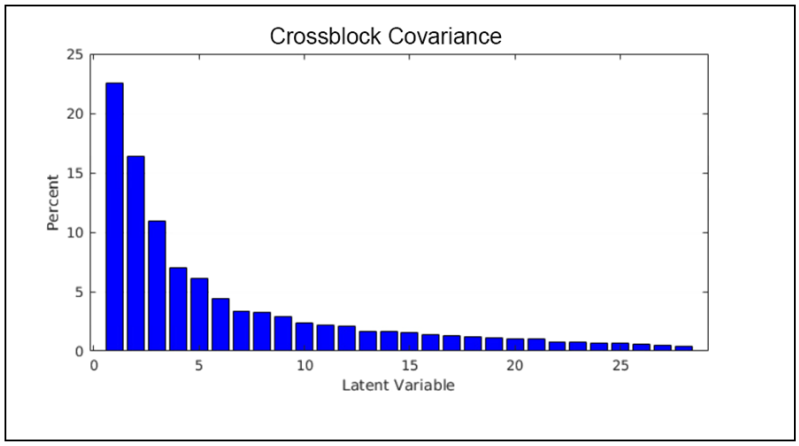

SF7. Associations between ventrorostral putamen functional connectivity and PLEs: LV1.

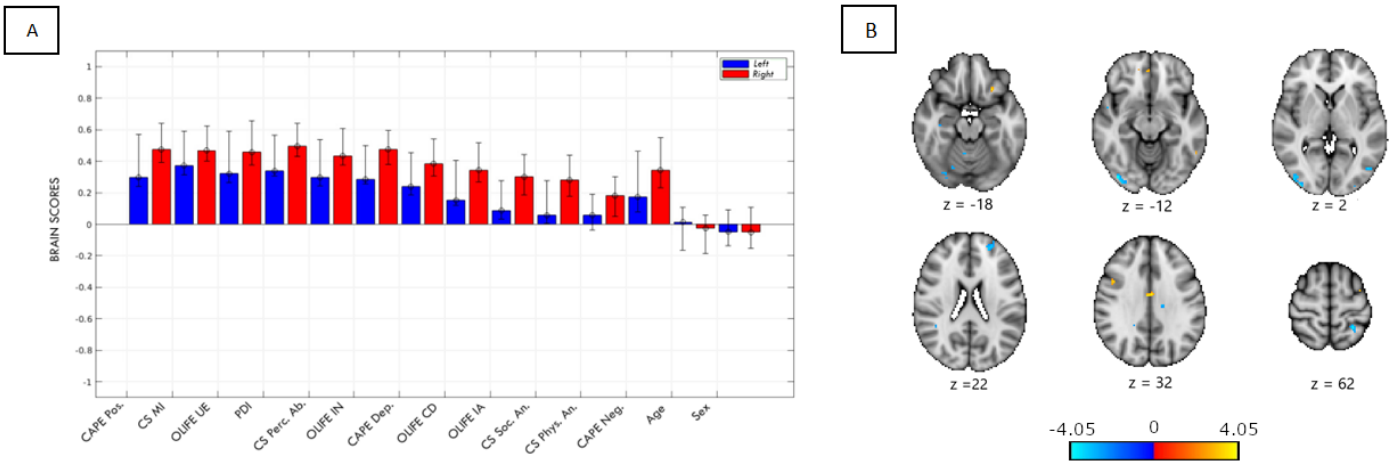

A: Correlations between each PLE scale, age, and sex and brain scores for LV1 in the PLS of ventrorostral putamen (vrPT) functional connectivity (FC). Error bars represent 95% confidence intervals. LV1 doesn't contains significant loadings from the PLE measures whose intervals cross zero. Blue: left vrPT seed-related FC: Red: right vrPT seed-related FC. B: Axial slices through the bootstrap image showing regions reliably contributing to LV1. Warm colours identify regions where vrPT-related functional connectivity was associated with the multivariate profile depicted in panel A (i.e., higher functional connectivity was associated with higher scores); cool colours show the opposite. Left hemisphere is on the left.
CAPE: community assessment of psychotic experience; sO-LIFE: Oxford-Liverpool Inventory of feelings and experiences short-form. PDI: Peters delusion inventory.

ST4 1 Cluster sizes and peak coordinates for bootstrap image of LV1, VRP analysis. Voxel mean: the average for all voxels in the cluster that passed the bootstrap ratio threshold.

		Peak Location						Bootstrap		Cluster size
Cluster#	Voxel Mean	X	Y	Z	X(mm)	Y(mm)	Z(mm)	BSR	Appro.P	(voxels)
1	0.000056384735	39	28	23	-14.0	-72.0	-28.0	40.524	0.0001	9
2	- 0.000019348039	24	55	24	-44.0	-18.0	-26.0	39.937	0.0001	6
3	0.000050235161	47	61	53	2.0	-6.0	32.0	39.384	0.0001	22
4	0.00011442236	56	72	43	20.0	16.0	12.0	38.548	0.0001	19
5	0.000071340051	43	76	57	-6.0	24.0	40.0	38.130	0.0001	11
6	- 0.000081413251	34	67	61	-24.0	6.0	48.0	37.949	0.0001	12
7	- 0.000026315574	59	76	28	26.0	24.0	-18.0	37.614	0.0002	8
8	- 0.000034463214	63	40	50	34.0	-48.0	26.0	36.066	0.0003	5
9	-0.00019769663	23	69	53	-46.0	10.0	32.0	35.346	0.0004	16
10	0.000012912966	26	85	39	-40.0	42.0	4.0	35.110	0.0004	6
11	- 0.0000052324008	34	25	42	-24.0	-78.0	10.0	34.756	0.0005	5
12	-0.00020185989	61	76	62	30.0	24.0	50.0	34.267	0.0006	9
13	-0.00014150515	44	87	31	-4.0	46.0	-12.0	33.368	0.0008	5
14	- 0.00024310324	66	40	39	40.0	-48.0	4.0	32.139	0.0013	5
15	- 0.0000025121335	26	22	33	-40.0	-84.0	-8.0	-44.638	0.0000	229
16	- 0.0000075471344	60	41	67	28.0	-46.0	60.0	-43.039	0.0000	30
17	0.000084259394	57	89	50	22.0	50.0	26.0	-40.534	0.0001	51
18	- 0.000032065302	36	28	29	-20.0	-72.0	-16.0	-39.241	0.0001	15
19	0.000022913986	39	39	22	-14.0	-50.0	-30.0	-39.129	0.0001	22
20	0.000035108529	26	43	45	-40.0	-42.0	16.0	-38.111	0.0001	21
21	- 0.00000053481835	59	51	59	26.0	-26.0	44.0	-37.926	0.0001	19
22	0.00012279610	27	42	17	-38.0	-44.0	-40.0	-37.630	0.0002	8
23	- 0.000010079778	68	24	32	44.0	-80.0	-10.0	-37.448	0.0002	7
24	- 0.0000078293424	31	32	35	-30.0	-64.0	-4.0	-36.761	0.0002	5
25	- 0.000039723989	27	82	33	-38.0	36.0	-8.0	-36.735	0.0002	14
26	- 0.000063053798	41	22	33	-10.0	-84.0	-8.0	-35.602	0.0004	9
27	- 0.000049977447	69	28	38	46.0	-72.0	2.0	-35.440	0.0004	19
28	-0.00016175539	34	23	55	-24.0	-82.0	36.0	-35.353	0.0004	6
29	- 0.00004290264	26	27	47	-40.0	-74.0	20.0	-34.327	0.0006	11
30	- 0.000076982717	59	30	33	26.0	-68.0	-8.0	-33.002	0.0010	5

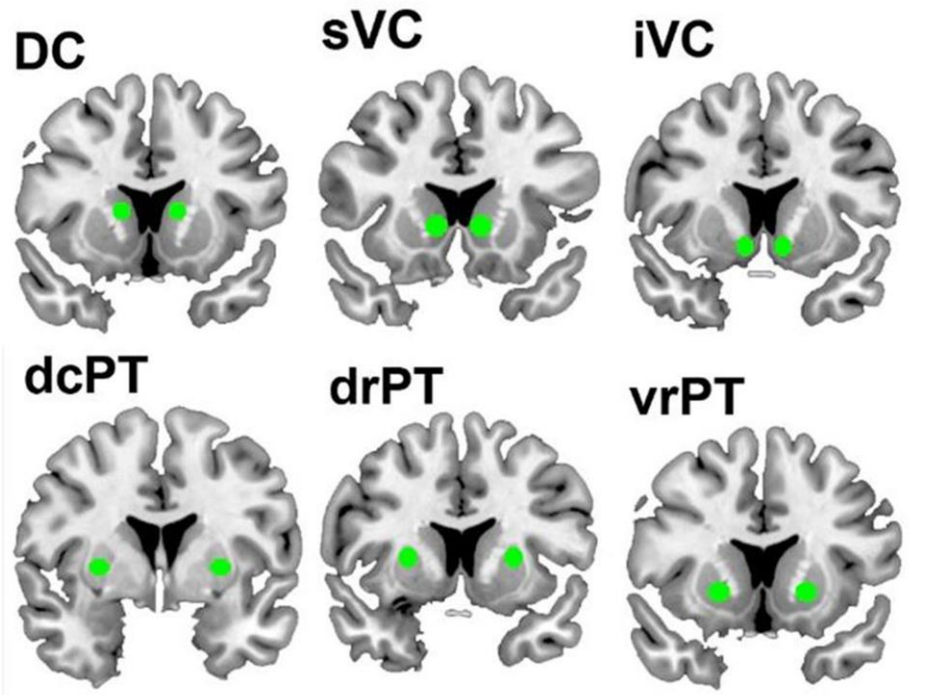

SF8. **Striatal seed regions-of-interest** (ROI). DC: dorsal caudate, sVC: superior ventral caudate, iVC: inferior ventral caudate, dcPT: dorsocaudal putamen, drPT: dorsorostral putamen, vrPT: ventrorostral putamen.

Measures of Psychosis-Like Experiences

The Oxford-Liverpool Inventory of Feelings and Experiences short-form (sO-LIFE)[1]**.** A shortened form of O-LIFE, a self-report measure of schizotypy traits in the general population. It is composed by 43 items covering four dimensions: Unusual Experiences (12 items), Cognitive Disorganization (11 items), Introvertive Anhedonia (10 items), and Impulsive Nonconformity (10 items). Yes/No response format, scored on a binary scale (0 = *'no'*; 1 = *'yes'*).

Peters Delusion Inventory 21-item (PDI-21)[2]**.** A self-report instrument assessing delusional ideation in the general population. It includes dimensions that measure distress, preoccupation, and conviction of unusual beliefs. To assess the presence of delusions in our sample, we used the PDI yes/no dimension. Total score ranging from 0 to 21, scored on a binary scale (0 = *'no'*; 1 = *'yes'*).

Community Assessment of Psychotic Experience (CAPE)[3]**.** This instrument, designed for the general population, it's a self-report measure (42 items) of subthreshold PLEs, evaluating positive (20 items), negative (14 items), and depressive (8 items) dimensions of these experiences. The frequency of experiences is measured by a 4-point Likert scale (1 = *'never'*; 4 = *'nearly always'*). By summing the scores of a subscale, it is possible to obtain a separate score for each dimension (maximum scores: 80 for the positive subscale, 32 for the negative subscale, 56 for the depressive subscale). Each of the three dimensions it's also accompanied by a distress scale, measured using a 4-point Likert scale (1 = '*not distressed'*; 4 = '*very distressed*').

Chapman Scales(Chapman and Chapman, 1980; Eckblad and Chapman, 1983). A series of four subscales that assess specific aspects of psychotic symptoms: the magical ideation scale (30 items), the perceptual aberration scale (35 items), the physical anhedonia scale (61 items), and the revised social anhedonia scale (40 items).

References

1. Fonseca-Pedrero E., Ortuño-Sierra J., Mason O. J. & Muñiz J. The Oxford-Liverpool Inventory of Feelings and Experiences short version: Further validation. Pers. Individ. Dif. (2015).
2. Peters E., Joseph S., Day S. & Garety P. Measuring delusional ideation: the 21-Item Peters et al. Delusions Inventory. Schizophr. Bull. 30, 1005–1022 (2004).
3. Mossaheb N. et al. The Community Assessment of Psychic Experience (CAPE) questionnaire as a screening-instrument in the detection of individuals at ultra-high risk for psychosis. Schizophr. Res. (2012).
4. Chapman L. J. & Chapman J. P. Scales for rating psychotic and psychotic-like experiences as continua. Schizophr. Bull. (1980).
5. Eckblad M. & Chapman L. J. Magical ideation as an indicator of schizotypy. J. Consult. Clin. Psychol. 51, 215–225 (1983).